DELIVERABLE REPORT

Deliverable:	D6.4: Identification of body target tissues accumulating MNMs
Work Package:	WP6: MNM bioavailability & biological affects in vitro/in vivo (ecotoxicology)
Lead Beneficiary:	Univerza v Ljubljani
Nature of Deliverable:	Report
Dissemination Level:	Public (PU)
Delivery Date:	31/08/2014
Submitted By:	Charles Tyler (UNEXE), Rhys Goodhead (UNEXE), Sara Novak (UNI-LJ), Damjana Drobne (UNI-LJ)
Revised By:	Katrin Volkmann (KIT), Silvia Diabaté (KIT), Paul Borm (N4I)
Approved By:	Eva Valsami-Jones (UoB)

Project full title: "Engineered nanomaterial mechanisms of interactions with living systems and the environment: a universal framework for safe nanotechnology"

Grant agreement no: NMP4-LA-2013-310451

Table of contents

1. Executive Summary

Here we applied a series of imaging methods to study the uptake and localisation of MNMs in the isopod, *Porcellia scaber,* and zebrafish, *Danio rerio*, as model test species, to facilitate studies into the bioavailability of MNMs to ecotoxicology-relevant targets. Atomic absorption spectrometry (AAS) and proton induced X-ray emission (PIXE) analysis were applied (UNI-Lj) to determine uptake and tissue concentration for silver and titanium dioxide MNMs and Coherent Anti stokes Raman Scattering (CARS) and whole mount *in situ* hybridisation (UoEXE) applied in zebrafish for studies on silver and cerium dioxide MNMs. The work on *P. scaber* established that TiO_2 MNMs did not accumulate in intact digestive gland cells, but silver did for animals exposed to Ag MNMs. For Ag MNM exposures, silver co-localised with Cu in metal storing granules of the digestive gland indicating that Ag^+ ions rather than Ag MNMs particles entered these cells. CARS microscopy was found to be a powerful tool for tracing uptake and distribution of MNM in exposed zebrafsh embryos. For exposures to Ag MNMs via the incubation medium we show that uptake was minimal due to particle aggregation and the low permeability of the chorion. The spatial resolution of CARS, however, did not allow for the tracing of single MNMs. Whole mount *in situ* hybridisation (WISH) in zebrafish embryos and early life stages with selected genes known to play key roles in metal trafficking and oxidative metabolism was shown to be highly effective for identifying target tissues for silver MNMs. The tissue affected included those involved in environmental sensing (olfactory bulbs and neuromasts) and ionocytes involved with ion transport. The gene responses associated with detoxification and oxidative stress, however, appeared to occur as a consequence of silver ions rather than a physical feature of the silver nanomaterials tested.

2. Introduction and current state of the art

One of the major challenges in studies into the biological effects of MNMs is developing understanding on their transport and subsequent fate in exposed organisms. An ability to identify body target tissues accumulating MNMs will inevitably help progress more targeted health effects analyses. The biological fate (bioaccumulation, body distribution, and cellular internalization) of different nanoparticles has furthermore become an important topic in risk assessment (Fabrega et al 2011). Bioaccumulation of metal nanoparticles can be studied by different techniques which provide data on the distribution and chemical state of elements in biological systems. Imaging techniques based on X-ray fluorescence currently rank among the most sensitive modalities for detection of elements in biological samples with submicrometer resolution. Proton induced X-ray emission (PIXE) is gaining importance in the analysis of elemental distribution and concentration in biological samples at the tissue level and delivers lateral resolution in the micron range (Vogel-Mikuš et al 2009). The prevailing technique used to study the body burden of Ag MNMs in organisms is atomic absorption spectrometry (AAS), which remains one of the most powerful methods for the analysis of metals in a wide variety of sample types (Bings et al. 2006). CARS microscopy offers many of the desired features for imaging uptake and fate of engineered nanoparticles, including the ability to image whole and sectioned cells with label free detection. Only recently however has it started to be applied to studies on MNMs. Another technique that offers potential in identifying target tissues for MNMs is whole-mount *in-situ* hybridisation (WISH) that can be applied to measure activation of selected genes associated with biological responses to MNMs.

Here we developed and applied some of the methods described above to study the uptake and localisation of MNMs in isopods, terrestrial invertebrates, and zebrafish, as a model fish test species. Atomic absorption spectrometry (AAS) and proton induced X-ray emission (PIXE) analysis were applied (UNI-Lj) to determine uptake and tissue concentration for selected MNMs and quantitative elemental concentration maps of biological tissue were produced in the isopod, *Porcellio scaber.* Coherent anti-Stokes Raman scattering (CARS) microscopy was applied to image particles in exposed zebrafish embryos and whole-mount *in-situ* hybridisation (WISH) with selected genes developed to investigate for target tissues of biological effect for Ag MNMs in early life stages (UEXE).

2.1 The study organisms

The terrestrial isopod, *Porcellio scaber*

Terrestrial isopods are a good choice for toxicity studies since oral uptake is the main route for contaminant intake and their accumulation in the body is attributed almost exclusively to dietary exposure (Drobne 1997). The digestive gland (hepatopancreas) cells are a major entity in the handling and processing of toxicants. They have an ability to assimilate high amounts of metals from the lumen of the gland (Hames & Hopkin 1989). Exposure of terrestrial isopods (prominently for *P. scaber*) to contaminant-treated food was established as a standard toxicity testing protocol by

Drobne and Hopkin (1994, 1995). Feeding exposure of *P. scaber* enables assessment of an exact exposure dose (Drobne 1997).

The zebrafish, *Danio rerio*

Zebrafish (*Danio rerio*) is a very useful model organism for investigations into the effects of MNMs in vertebrate systems. It is highly researched with respect to developmental processes and there is a plethora of supporting literature. Zebrafish embryos offer a wide range of experimental conveniences, including the ease for observing developmental effects through a transparent chorion and body up until 48 hours post fertilisation (hpf). Additionally, the fish/embryo are cultured easily and high replication is possible using embryos. Exposures can also be undertaken via the water or via microinjection. For gene work this is facilitated by the availability of a sequenced genome.

2.2 Atomic absorption spectroscopy

Atomic absorption spectrometry (AAS) is an analytical technique for qualitative and quantitative determination of chemical elements. AAS enables determination of more than 70 elements (mostly metals and metalloids) in very low concentrations (in the ppm range, i.e. mg/kg or mg/L). The accuracy is very good; the extent of measurement error is about 1-2%. Flame AAS (FAAS) is one of four commonly used AAS techniques, others being graphite furnace AAS (GF-AAS), inductively coupled plasma optical emission spectroscopy (ICP-OES) and inductively coupled plasma mass spectrometry (ICP-MS).

FAAS is based on the fact that metal atoms in the ground state absorb light of specific wavelengths. Analytes of interest needs first to be atomized in a flame. A beam of light of a suitable wavelength (in the ultraviolet or visible region of the spectrum) passes through the nebulized sample and converts atoms of the analyte to the excited state. Characteristic excitation wavelengths are specific to each element and precise to 0.01-0.1 nm. Concentration of the element in the sample is determined from the absorption rate, which is compared to the working curve obtained after calibrating the instrument with standards of a known concentration. FAAS is a monoelemental technique. A drawback of AAS techniques is they do not provide localisation at a cellular resolution.

2.3 Proton induced X-ray emission (PIXE) analysis

In the literature, a variety of methods have been used to study cellular/tissue internalization and body distribution of MNMs. Proton induced x-ray emission (PIXE), is a powerful yet non-destructive elemental analysis technique and is frequently used for biological samples. One of the major advantages of this method is in its high sensitivity (to ppm level measurements for certain elements). It is multi-elemental method; up to 20 elements can be determined simultaneously, but is not as sensitive for higher-Z elements. It allows the investigation of chemical-free prepared samples up to 50 µm thick. The results of PIXE measurements are quantitative elemental concentration maps of biological tissue. Maps of element distribution can provide valuable

information that is not possible to obtain using point analyses or linear scans (Vogel Mikuš et al 2009).

2.4 Coherent anti-Stokes Raman scattering (CARS) microscopy

Techniques applied for the quantification of MNM uptake in biological systems have included inductively coupled plasma mass spectroscopy (ICP-MS) and single nanoparticle (SN ICP-MS) on tissue extracts (Ferry et al., 2009; Scown et al., 2009). Radioactively labelled MNMs have been used to trace MNM transport and tissue localisation (Lu et al., 2010; Sumner et al., 2010). More recently, stable isotope tracing has been used for the detection of metal based nanomaterials in samples with high natural background levels of the respective elements (Larner et al., 2012). Although these techniques potentially enable accurate quantification of MNM distribution, the particles can be localised only to the tissue or organ. Direct imaging techniques on the other hand offer powerful methods for visualising MNMs within tissues, at cellular and even sub-cellular levels. There are few well-defined techniques, however, for accurately imaging or characterising nanoparticles within a biological matrix. Electron microscopy (EM) has sufficient resolution to determine nanoparticle localisation within in a tissue (Cheng et al., 2007; Mouchet et al., 2008; Soto et al., 2005), and high-resolution transmission electron microscopy (TEM) can provide detailed information on the structure of individual nanoparticles (Petri-Fink et al., 2008). EM techniques can also be combined with energy-dispersive X-ray spectroscopy (EDX) analysis to identify the nature of any metal constituents of the MNMs. However, samples for both TEM and Scanning Electron Microscopy (SEM) require preparation methods and imaging conditions which can create artefacts within the sample, such as MNM aggregation, that do not have an exposure related aetiology. These techniques also do not allow for imaging of live tissues. Furthermore, TEM can generally only be used for metallic particles that are electron dense as non-metal coatings or shells lack adequate contrast (Fan et al., 2007).

Confocal microscopy, a linear optical technique has been applied successfully to visualize the bio-distribution multi-walled carbon nanotubes (MWCNTs) in zebrafish (*Danio rerio*) embryos (Cheng et al., 2009b) and polystyrene nanoparticles in hepatocytes (Johnston et al., 2010). The disadvantage of standard confocal microscopy, however, is the requirement to stain the sample to provide contrast or, fluorescently label the nanoparticles (as in the studies of Cheng et al., 2009a; Johnston et al., 2010), which may change the nature of the particle (including their toxicity). Confocal techniques also lack spatial resolution (approximately 0.5 µm) and although they have sufficient depth penetration for studies on cultured cells, they are limited in depth penetration for most applications on whole tissues and *in vivo* imaging.

In theory, CARS microscopy offers all of the desired features for imaging uptake and fate of engineered nanoparticles, including high selectivity (or contrast) and high sensitivity for NMs, the ability to image whole and sectioned cells, an ability to visualise cell structure, label free detection, non-invasive, yield complimentary chemical information, high accuracy, reproducibility and high throughput.

A fundamental requirement for the imaging of MNMs within tissues is the ability to identify the structures of the biological materials themselves, the tissues, cells, and cellular components. This information is clearly required to localise the MNMs within the tissue matrix before any measurements, comparisons, aberrations or diagnostic data can be drawn. Utilising the variation in intrinsic biochemical properties of a tissue/cell, CARS enables visualisation of a range of structural features. As the contrast is provided by the chemical composition of the biological sample (i.e. what bonds are targeted), CARS images provide more information than a corresponding transmitted light image. This range of chemical selectivity is demonstrated with the excitation and identification of phosphate groups, C-O bonds of DNA, C=C and C-H bonds, and amide bonds (Cheng et al., 2002a; Cheng et al., 2002b; Hashimoto et al., 2000; Volkmer et al., 2001). This enables imaging of subcellular structures such as the nucleus (see Figure 2b, c & 4a), without the need for any non-native contrast agent or pre-processing of the sample which could interfere with endogenous biological processes of interest. An important point to note, however, is that when using CARS to image a particular molecular species, these functional groups will appear in a variety of different biomolecules, and the image will thus require further information or interpretation to clarify precise localisation.

2.5 Whole mount in-situ hybridisation (WISH)

Standard approaches for testing the effects of nanoparticles do not inform on material partitioning within the body or the target organs affected in an integrated manner. WISH as applied to zebrafish embryos and early life stages potentially offers a highly integrative, systems-wide approach to assess the toxicity of nanoparticles through effects on gene expression. The method offers the ability to target where in the body nanomaterials induce biological responses to help inform on their potential health effects. Application of the technique of in situ hybridisation to assess for effects of toxicants on target genes, however, requires understanding on the ontogeny of the expression of the target genes, and this is known for very few genes of specifically nanotoxicological relevance.

Original methods for ISH developed in the 1980s, used radioactively labelled DNA probes to detect expression of genes on histological sections. In the 1990s, the use of chemically labelled antisense RNA probes allowed analysis of whole-mount tissues or embryos making the analysis of gene expression patterns quicker, safer and easier.

The WISH technique has several important applications: it allows gene expression profiles in cells, tissues and organs to be determined during the time course of embryo differentiation. Collections of tissue and cell-type-specific markers at distinct developmental stages can be assembled by implementing an ISH screen and these markers can be used for phenotypic analysis after experimental manipulation of embryos or after exposure. Identification of similar spatial and temporal expression patterns by ISH is a reliable method to define genes that may not be physically linked, but are involved in the same process and are coordinated in their expression.

WISH provides a quick and efficient method to establish spatial and temporal gene expression patterns in embryos and early larvae. Although expression in trunk and tail tissues, especially notochord and myotomes, is increasingly difficult to visualize by WISH as the embryo gets older, this technique works very well for visualizing gene expression in endodermal derivatives and in sensory organs during late embryogenesis and early larval stages. Current alternative options to determine the expression of genes is to look at the localization of the corresponding protein using specific antibodies. The main disadvantage of this method is that, for each protein, a specific antibody has to be generated and the conditions for immunohistochemistry have to be defined each time (fixation, dilution, detergents, washes). This becomes a slow process limiting the number of probes able to be used at the same time.

Objectives

Identification of body target tissues accumulating MNMs in the terrestrial isopod, *P. scaber* and in zebrafish, *Danio rerio* embryos/early life stages.

3. Experimental approaches

3.1 Porcellio scaber

3.1.1 Feeding experiments

Terrestrial isopods *P. scaber* (Isopoda, Crustacea) were collected during different periods at uncontaminated locations in Slovenia. The animals were kept in a terrarium filled with a layer of moistened soil and a thick layer of partly decomposed hazelnut tree leaves (*Corylus avellana*), at a temperature of 20 ± 2°C and a 16:8-h light:dark photoperiod.

In the feeding experiment the animals consume MNMs applied in a suspension on the dried hazelnut leaf (*Corylus avellana*). Only adult animals of both sexes and weighing more than 30 mg were used in the experiments. A suspension of particles or distilled water was brushed onto the lower leaf surface of the leaves and left until dry. Each individual animal was placed in a Petri dish and one hazelnut leaf was the animal's only food source. Humidity in the Petri dish was maintained by spraying tap water on the internal side of the lid every day. All Petri dishes were kept in a large glass container under controlled conditions in terms of air humidity, temperature (21 ± 1°C), and light regimen (16:8h light:dark photoperiod).

Animals in each individual experiment were exposed to varying concentrations of MNMs for 14 days or for different periods in the case of females with marsupial (containing developing eggs). The initial number of animals tested was selected on the basis of the type of analyses conducted after exposure. After the exposure, the animals were anesthetized at a low temperature and then decapitated and their digestive glands and gut isolated. Also whole animals were used for further analyses.

After the exposure, the faecal pellets and leaves were removed from the Petri dishes, air dried, and weighed separately. The feeding rate of isopods was calculated as the mass of consumed leaves per animal's wet weight per day. The food assimilation efficiency was calculated as the difference between the mass of consumed leaves and the mass of faecal pellets divided by the mass of consumed leaf. The amount of MNMs consumed was calculated on the basis of the quantity of leaf consumed and the amount of MNMs applied on the leaf, with the assumption that the suspension is applied evenly on the leaf surface.

3.1.2 Sample preparation for AAS measurements

After feeding experiments animals were anesthetized at a low temperature and then decapitated and their digestive glands and gut isolated. Samples of glands, gut and rest of the animal's body were lyophilized, weighed, and completely digested in an acid. Digestions were carried out with the aid of a wide variety of reagents. Aside from the various mineral acids, other reagents such as hydrogen peroxide, potassium peroxide sulfate, boric acid, and many more were also employed. The selection of the specific reagents or the preparation of a reagent mixture depended on the sample digested. Organic sample materials are generally decomposed to carbon dioxide with the aid of oxidizing acids (primarily nitric acid) and reagents (primarily hydrogen peroxide) and completely mineralized. Acid digestion enables destruction of organic molecules, solubilization of the analyte and simplification of analyte matrix, which is a prerequisite for measurements with AAS. We implemented microwave acid digestion of organic material instead of open digestion in a recycling device or with the traditional "hot plate". While operating temperatures in open systems are limited by the boiling point of the acid solution, closed digestion vessels typically allow temperatures in the range of 200–260 °C to be reached. This results in a dramatic increase in the reaction kinetics, allowing digestions to be carried out in a matter of hours or even minutes. After digestion of samples, residue are taken up in HNO_3 and total element concentrations in the tissue were determined by AAS. Reagent blanks and standard solutions were used to ensure accuracy and precision in the analysis.

3.1.3 Sample preparation for PIXE

After feeding experiments, digestive glands or whole animals were shock-frozen in liquified propane or liquid N2, using tissue-freezing medium (Jung Tissue Freezing Medium, Leica). Samples were then sectioned at 60 µm using a Leica CM3050 cryotome with the temperature of the microtome head and chamber maintained between -28°C and -20°C. The sections were placed in pre-cooled Al holders, transferred to an alpha 2–4 Christ freeze dryer using a cryotransfer assembly, cooled with liquid nitrogen, and then freeze-dried at -30°C and 0.4 mbar for 24 h. Dry sections were mounted between two thin layers of Pioloform foil on the Al sample holder.

Measurement of micro-PIXE and data evaluation for the isopod samples at the micro-PIXE laboratory at the Jozef Stefan Institute in Ljubljana has previously been described in our publications previously (Novak et al 2012, Pipan Tkalec et al 2011).

The micro-PIXE method at Jozef Stefan Institute also enables examination of frozen-hydrated tissue samples. Frozen-hydrated sample preparation has several advantages; the preparation of sample and sample mounting procedure to the sample holder is less delicate, the preparation process is shorter and consequently there are less possible artefacts in the sample. The temperature of the cold stage in the measuring chamber was kept below 130 K throughout the entire proton beam exposure.

We compared biological tissue samples prepared in frozen-hydrated state and freeze-dried state and observed significant differences in elemental distribution of particular elements. We adapted the cryofixation method for micro-PIXE for *Porcellio scaber*.

3.2 Danio rerio

3.2.1 CARS Imaging experiments

CARS was applied as a method in zebrafish embryos to both measure the intrinsic biodistribution of nanoparticles (through microinjection studies) and to assess for uptake from the natural culture environment (MNMs dosed into the culture medium).

The MNMs used for this work were cerium (IV) oxide with a primary crystal size of 10.3 nm (NM212) and silver MNMs with a diameter of 15 nm (NM-300K). Both MNM types were acquired through the NanoMILE consortium.

In the case of dosing MNMs in culture medium for studies on their uptake into fish embryos, there is a propensity for nanoparticles to agglomerate in aquatic media, which has not been fully characterised. As a consequence bioavailability of nanoparticles to aquatic organisms is likely to be very different from the nominal dose. Additionally, aggregation away from the nanoscale is likely to vary with temperature, pH, ionic strength, presence of humics etc. It was decided therefore for the first set of studies to circumvent this problem and directly inject MNMs into embryos to assess the ability for tracing MNMs via CARS in zebrafish embryos.

For the microinjection work zebrafish embryos were collected from group spawning WIK/wild-type adults, cleaned and placed into a petri-dish for microinjection. Embryos were handled gently with forceps and maintained in a fixed position using a conduit created with a microscope slide. Eggs were lined up with the animal pole facing outward, allowing microinjection into the cell with minimum damage. Microneedles (1 mm O.D., 0.58 mm I.D.) were pulled using a Narishige PC-10 puller. The appropriate injection volume is about 10–20% of that of the cytoplasmic volume, which is about 10 nl for the one-cell stage. Larger volumes can burst cells or cause nonspecific deformity of the embryos. 1 nl can theoretically contain 1 million billion spherical (d. 1nm) nanoparticles.

Embryos were incubated for designated periods (6, 24, 48 hours) before being imaged with the CARS system. In the instance of imaging at 48 hours phenylthiourea (PTU) was trialled as a pigment supressing chemical, from 12 hpf until sampling, to maintain the transparency of embryos beyond 24 hours, after which iridophore and melanophore pigment cells begin to develop and complicate spectral assignment of the CARS signals. Embryos were immobilised with benzocaine before imaging commenced.

In a further series of studies, exposures to MNMs were conducted via the embryo culture medium. These studies were conducted to assess for natural behaviour and uptake of selected MNMs into exposed embryos from the culture environment using CARS.

3.2.2 CARS set-up

CARS imaging was performed using a custom-built microscopy system based on a commercial confocal laser-scanning microscope (IX71 and FV300, Olympus UK) and a synchronized dual-wavelength picosecond laser source (Figure 1). Laser excitation was provided by an optical parametric oscillator (OPO) (Levante Emerald, APE, Berlin) pumped with a frequency doubled Nd:vandium picosecond oscillator (High-Q Laser Production GmbH). The pump laser generated a 6 ps, 76 MHz pulse train at 532 nm with adjustable output power up to 10 W. The OPO produced collinear signal and idler beams with perfect temporal overlap and provided continuous tuning over a range of wavelengths. The signal beam was used as the pump, ranging from 670 to 980 nm and fundamental of Nd:vanadium (1064 nm) used as the Stokes beam. The maximum combined output power of the pump and Stokes was approximately 1 W, which was attenuated to reduce the power at the sample to between 15 and 30 mW. To improve the transmission of the near-IR excitation through the commercial microscope, the galvanometer mirrors were replaced with silver mirrors and the tube lens was replaced with a MgF2 coated lens. The collinear pump and Stokes beams were directed onto the scanning confocal dichroic which was replaced by a silver mirror with high reflectivity throughout the visible and NIR (21010, Chroma Technologies, Bellows Falls, VT). The forward-CARS signal was collected by the air condenser, transmitted by the dichroic mirror and directed onto a red-sensitive photomultiplier tube (R3896, Hamamatsu Photonic UK). The epi-CARS signal was collected using the objective lens and separated from the pump and Stokes beams by a long-wave pass dichroic mirror (z850rdc-xr, Chroma Technologies) and directed onto a second R3896 photomultiplier tube at the rear microscope port. The CARS signal was isolated at each photodetector using a single band-pass filter centered at the anti-Stokes wavelengths. Imaging was performed using either a 60× water immersion, or 20× air objective (UPlanS Apo, Olympus UK).

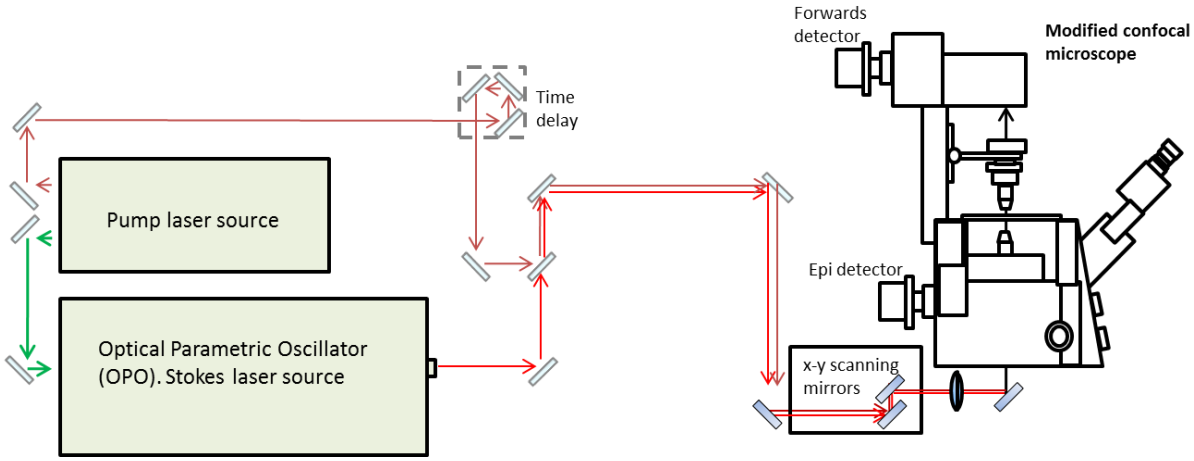

Figure 1. Schematic diagram of CARS set-up.

Features of the CARS process can amplify various components of MNMs that facilitate specific imaging of the material. Although some non-resonant contributions reduce image contrast some, however, are useful. Materials with naturally large non-resonant susceptibilities provide excellent contrast using CARS spectroscopy. This is due to their strong electronic resonances, which generate extremely strong forwards and backwards (F- and Epi-CARS respectively) detected signals. This occurs for metal oxide MNMs, as demonstrated by Moger et al. (2008). In addition to exhibiting markedly different chemical properties from their bulk materials, MNMs can also exhibit enhanced optical properties that are often accompanied by an enhancement of the nonlinear optical properties. Moger et al. (2008) showed that this enhancement can be exploited in metal oxide MNMs to produce large signals, thus allowing excellent visualisation of these materials. The heightened nonlinear response of some NMs allows for the location of particles far smaller than the linear scaling of the signal from bulk material would suggest. CARS images were recorded in 2 or 3 channels, both F-CARS and backwards Epi-CARS detected signals or stimulated Raman scattering (SRS) combined with Epi-CARS, with a transmitted light channel sometimes recorded.

3.3 WISH experiments

WISH was conducted on zebrafish embryos exposed to citrate-covered Ag 10-nm MNMs (measured diameter of 9.9 ± 3.1 nm; AgNPCi) and larger sized (bulk) citrate-covered Ag particles (measured diameter of 160 nm AgBCi), acquired from the University of Birmingham. Uncoated silver MNMs with a diameter of 15 nm (NM-300K) were acquired through NanoMILE, uncoated Ag bulk (measured diameter of 137 ± 62.0 nm; AgB) bulk were acquired from Nanostructured and Amorphous Materials Inc. Houston, USA. $AgNO_3$ was dosed at a level calculated to provide an approximate dissolution equivalence (1-2%) for the dosing of AgNPCi, based on previous dissolution experiments with these materials, exposure medium and exposure periods (Osborne et al., 2012).

Heavy metals, including silver, induce oxidative stress in a wide range of organisms spanning algae to fish and usually they do so via generation of reactive oxygen species (ROS) resulting in lipid

peroxidation. Ag MNMs have been shown to induce oxidative stress *in vitro* through an increase in the production of ROS. In their detoxification in the body, metals usually bind to thiol-containing compounds such as metallothionein (MT) and glutathione (GSH, (Mason and Jenkins, 1995; Maracine and Segner, 1998).

WISH was applied in zebrafish embryos and early life stages exposed to Ag MNMs, a bulk counterpart and silver ions, for a suite of genes known to respond to metals (toxicity, transport and storage), oxidative stress and other markers of cellular stress. The genes selected were metallothionein (*mt2*), glutathionine S-transferase pi (*gstp*), glutathionine S-transferase mu (*gstm1*), heme oxygenase (*hmox1*) and ferritin heavy chain 1 (*fth1*). *Mt2* is involved with transport and storage of heavy metals (Andrews, 2000) and has been shown previously to be responsive to Ag MNMs in zebrafish embryos (Osborne et al., 2012). Glutathionine S-transferases are a major group of detoxification enzymes that catalyze the nucleophillic addition of the tripeptide GSH to many xenobiotics and endogenous electrophiles. Gstm1 functions in the detoxification of electrophilic compounds and *gstp* plays roles in xenobiotic metabolism and oxidative stress (Garner and Di Giulio, 2012). Gstp is also known to be responsive to silver (Cheng et al., 2006). The *gstm1* gene encodes for the carcinogen detoxification enzyme glutathione S-transferase M1. Heme oxygenase (encoded by *hmox1*) is an enzyme that catalyzes the degradation of heme which in turn produces iron and protects against oxidative stress (Ponka et al., 1998). We initially studied the ontogeny and tissue expression profiles for each of these target genes in unexposed animals up to 12 days post fertilization (dpf) to determine their expression dynamics and identify the most appropriate life stages for studies on the effects of silver materials. Antisense RNA gene probes for *mt2, gstm1, gstp, hmox1* and *fth1* were synthesised by PCR from cDNA (Osborne *et al*., 2012).

For the hybridizations, embryos were fixed using 4% PFA in PBS at 4ºC overnight. They were then dechorionated and placed in methanol for 2 hours. Embryos/larvae were incubated in proteinase K (5µg/ml) for either 30 minutes (for embryos between 24 hpf to 5 dpf) or 40 minutes (for larvae between 6 dpf and 12 dpf). They were then washed two times with PBS+0.1% Tween 20 (PBSTw), placed in hybridisation buffer for 1 hour and incubated with the desired probe overnight at 65ºC. Embryos were then washed in 50% formamide 2XSSC, 0.1%Tween 20for 30 minutes at 65ºC, followed by a 2X SSC 0.1% Tween 20 wash at 65ºC and received 2x 30 minutes washes at 65ºC with 0.2X SSC 0.1%Tween 20. Blocking solution (2% blocking reagent containing 2.5 ml of calf serum in maleic acid based buffer (MAB)) was added and the embryos were incubated for 1 hour at RT. Anti-DIG antibody (5000x diluted with blocking solution) was then added and the embryos incubated for 2 hours at room temperature. Embryos subsequently received a series of 4 x 30 minutes washes in PBSTw before a 10-minute wash with AP (alkaline phosphatase) buffer (Tris 0.1 M pH 9.5, NaCl 0.1 M, MgCl2 50 mM, Tween 20 0.1%). Embryos were transferred to a 24 well plate and placed in staining solution (chromogenic BM-Purple AP Substrate, Roche) to reveal the probe, and photographed using a Nikon SMZ1500 stereo microscope equipped with a digital camera. For the studies on gene ontogeny, the levels of gene expression were assessed on a qualitative basis. For the silver materials exposure work the levels of expression of the different genes studied were quantified using Image-J 1.44 P. Here, the expression intensity for a target gene was determined for

a specific tissue area for 15-20 embryos/larvae, subtracting any background. The intensity value obtained was then converted to a fold change (FC) compared with controls to give an approximate quantification of effect for the different silver material treatments for that gene and tissue. Given the variation in the background expression of the target genes, only measured expressions differing from controls by more than 20% (i.e. fold changes above 1.2 or below 0.8) were considered as significant.

4. Results and Discussion

4.1 P. scaber

After several preliminary experiments where animals were exposed to different TiO_2 MNMs, elemental analyses using PIXE was performed on the digestive gland tissue of animals in order to observe possible bioaccumulation of MNMs in the tissue, but no Ti was detected.

In preliminary experiments dosing isopods to Ag MNMs via food, elemental analysis subsequently showed presence of Ag ions in the digestive gland epithelium of exposed animals. Silver co-localised with Cu in metal storing granules and thus Ag ions rather than Ag MNMs particles had entered the cells (Figure 2).

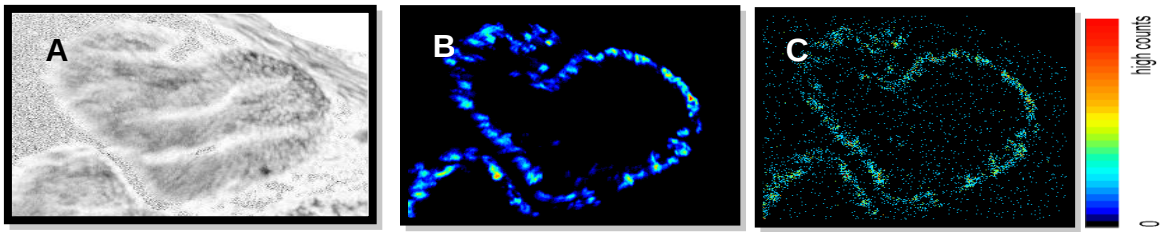

Figure 2. Micro-PIXE qualitative elemental maps of digestive gland of animal exposed to food dosed with 5000 µg nano-Ag/g dry weight of food. (B) Elemental map of Cu (B) and (C) elemental map of Ag (C).

A further exposure study was conducted with Ag MNMs (received from project partner - JRC, internal code Ag_90). In this experiment there was no effect on feeding rate, weight change and mortality of the exposed animals.

Results of elemental analyses of different body fractions (digestive glands, gut and the rest of the body) with atomic absorption spectroscopy showed that Ag accumulated in hepatopancreas of animals and not in the gut or the rest of body. Ag was also found to accumulate in the hepatopancreas, gut and rest of the body of animals for animals exposed to $AgNO_3$ (Figure 3).

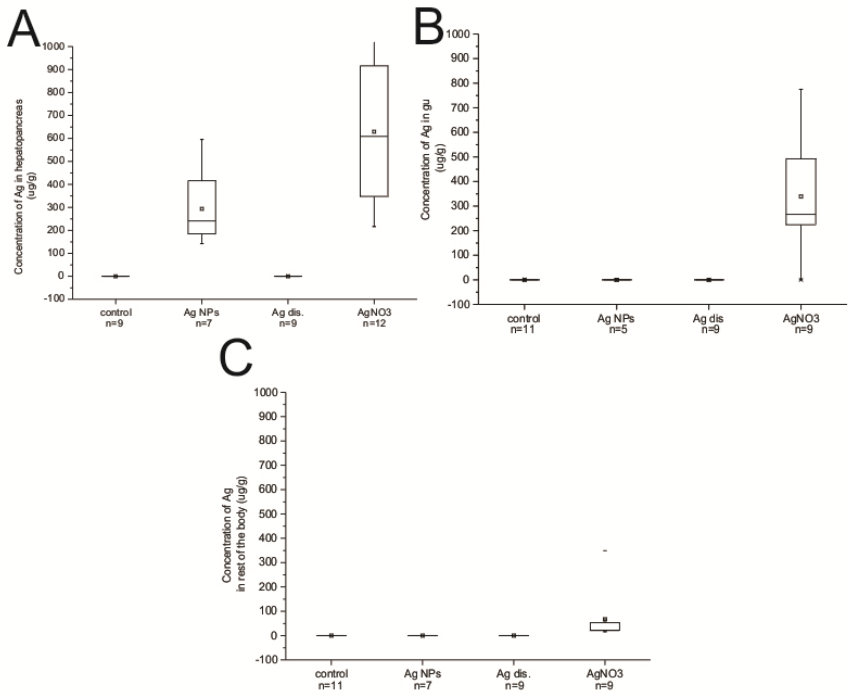

Figure 3. (A) Concentration of Ag in hepatopancreas of animals exposed to Ag MNMs, Ag dispersant or $AgNO_3$, (B) Concentration of Ag in gut of animals exposed to Ag MNMs, Ag dispersant or $AgNO_3$, (C) Concentration of Ag in rest of the body of animals exposed to Ag MNMs, Ag dispersant or $AgNO_3$. Symbols on the box plot represent minimum and maximum data values (whiskers), mean value (□), 75^{th} percentile (upper edge of box), 25^{th} percentile (lower edge of box), median (line in box) and max and min value (-).

Samples from this exposure have been prepared for PIXE analyses and analyses are in progress.

4.2 Danio rerio

4.2.1 CARS

Understanding of the CARS output is of vital importance for image interpretation. Subsequent contrast superimposition to understand what effects are illustrated within the image, such as the biodistribution or penetrance of MNMs, requires intelligent processing by the user that is sensitive to the original image. As both chemical and structural detail are generated, visual information from biological structure must be correlated to tissue or cell type and be cognisant to the tuned excitation wavelength.

Precise localisation of MNMs within a biological matrix is extremely useful for risk assessment but is demanding for the imaging technique. The first challenge is having sufficient spatial resolution to locate particles within a cell and is ideally combined with a 3-dimensional sectioning capability. We found that the CARS signal is sufficiently precise to be able to allow this. The second major challenge is that the imaging modality can detect and derive sufficient contrast from both the biological matrix and the MNMs, which are highly varied targets. Important in this respect is the accuracy of CARS

imaging compared to tracing MNM localisation using fluorescent tags or markers. This is because CARS directly images the particle itself and not the label attached to aid its tracking, as some other microscopy methods require, ensuring determination of the precise localisation of a MNM. Potentially where tracers/fluorescent markers are used, the label can become dissociated from the particle giving a false positive signal. As an example of this, in a study by Xu et al (2008) a lipophilic dye was shown to be released from nanoparticles into the surrounding extracellular medium before the dye was taken up by cells. In this instance confocal microscopy and data from a fluorescence activated cell sorter (FACS) produced data that suggested nanoparticle uptake, yet CARS assessment showed the absence of particles within the cells, giving a different conclusion; indicating a lack of nanoparticle uptake.

We have exploited the FWM process of CARS when imaging MNMs within a biological matrix, to distinguish the MNM's non-resonant susceptibilities from the stimulated vibrational contrast from commonly targeted molecules such as lipids. Thus, the ability to tune the excitation wavelength away from the natural vibrational resonance of a sample (used for structural information), allows for confirmation of the presence of MNMs which produce a strong signal across a broad wavelength spectrum. This is because the C-H bonds will not produce non-resonant contributions in the image (Akimov et al., 2009) and off resonance, in the biologically silent region of the Raman spectrum, the only signal generation will come from the MNMs.

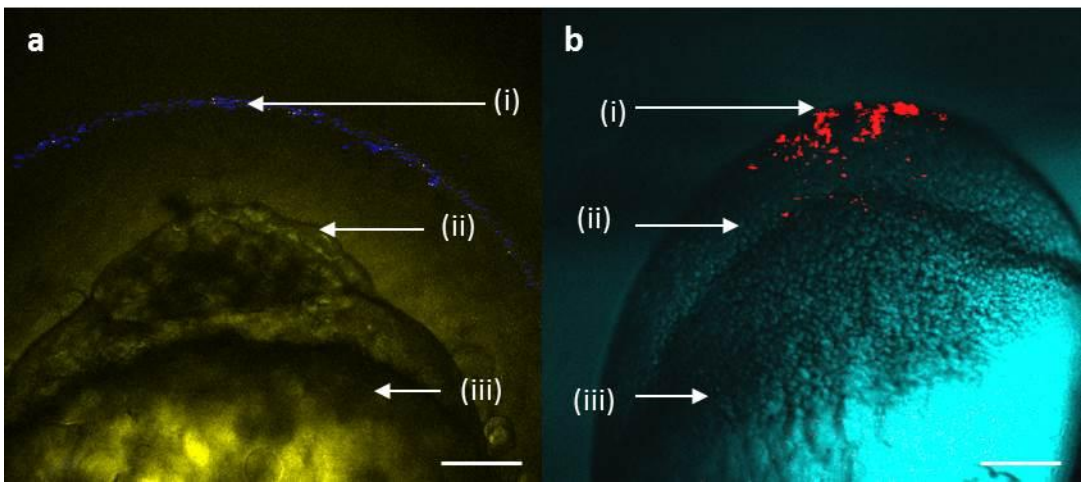

Figure 4. Zebrafish embryos microinjected at the 1 cell stage with (a) CeO_2 nanoparticles (i, contrasted blue), imaged 3.5 hpf and (b) Ag nanoparticles (i, red) imaged 6 hpf. Both images are visualised at 2850 cm^{-1} the CH_2 excitation frequency. (ii) Indicates the mass of dividing cells and (iii) the yolk. Scale bars represent 100 µm.

We have used this ability to distinguish MNM from biological material by tuning the excitation wavelength off resonance for C-H bonds to confirm the remaining signals were derived from MNMs.

This tuning method of CARS removes the possibility of confusion between native and non-native scatterers, such as lipids and NMs respectively within the sample. This technique can be applied for any MNM within the system, although, particles that require exploitation of their specific properties,

will only be visible at their particular stimulated wavelength. An example of this is for gold nano-shells (Garrett *et al.*, 2011).

It should be stated that the CARS process is principally qualitative and a notable drawback is that the CARS signal does not scale linearly with compound concentration making quantitative analysis problematic, although not impossible. Quantitative capabilities of CARS are most limited with less abundant scattering targets.

The use of live samples can exhibit all the biological processes that interact with or are stimulated by the presence of MNMs. This makes real-time imaging a perfect snap-shot of the true functionality and behaviour of the MNMs in situ and additionally the same sample can be imaged at different time points of exposure.

Studies on microinjected zebrafish embryos initially focused on very early cell division and the biokinetics of MNMs from the single cell to the developing deep cell layer. Here we compared different MNM types. Figure 4 shows embryos that where microinjected with CeO_2 MNMs or Ag MNMs. CeO_2 MNMs injected into the 1 cell stage of zebrafish embryos associated with the chorion (Figure 4a) and were not observed to be retained in the embryo at 3.5 hpf (hours post fertilisation). This was not the case however for Ag MNMs (15 nm, Figure 4b), which were seen to remain internalised in the embryo structure and integrated throughout dividing cells at 6 hpf. This shows a clear variation in behaviour between the two particle types and this is likely to have a significant bearing on any toxicological responses they might induce.

Limitations of CARS technique for tracing MNMs that particularly apply to the imaging of whole organisms include the size of the target that can be screened and the opacity of its surface. Some organisms such as zebrafish contain pigment cells, including melanophores and iridophores, which limit imaging of embryos past 25 hpf. This is because the signals from the developing pigments are indistinguishable from the broad signal wavelength from many metal MNMs. To counter this we exposed zebrafish embryos from 12 hpf with phenylthiourea (PTU) until 48 hours (Figure 6). Although the suppression of pigment development was successful (Figure 6) and CARS images were obtained (Figure 5a) treatment of the embryos with PTU could potentially affect MNM uptake from the incubation medium.

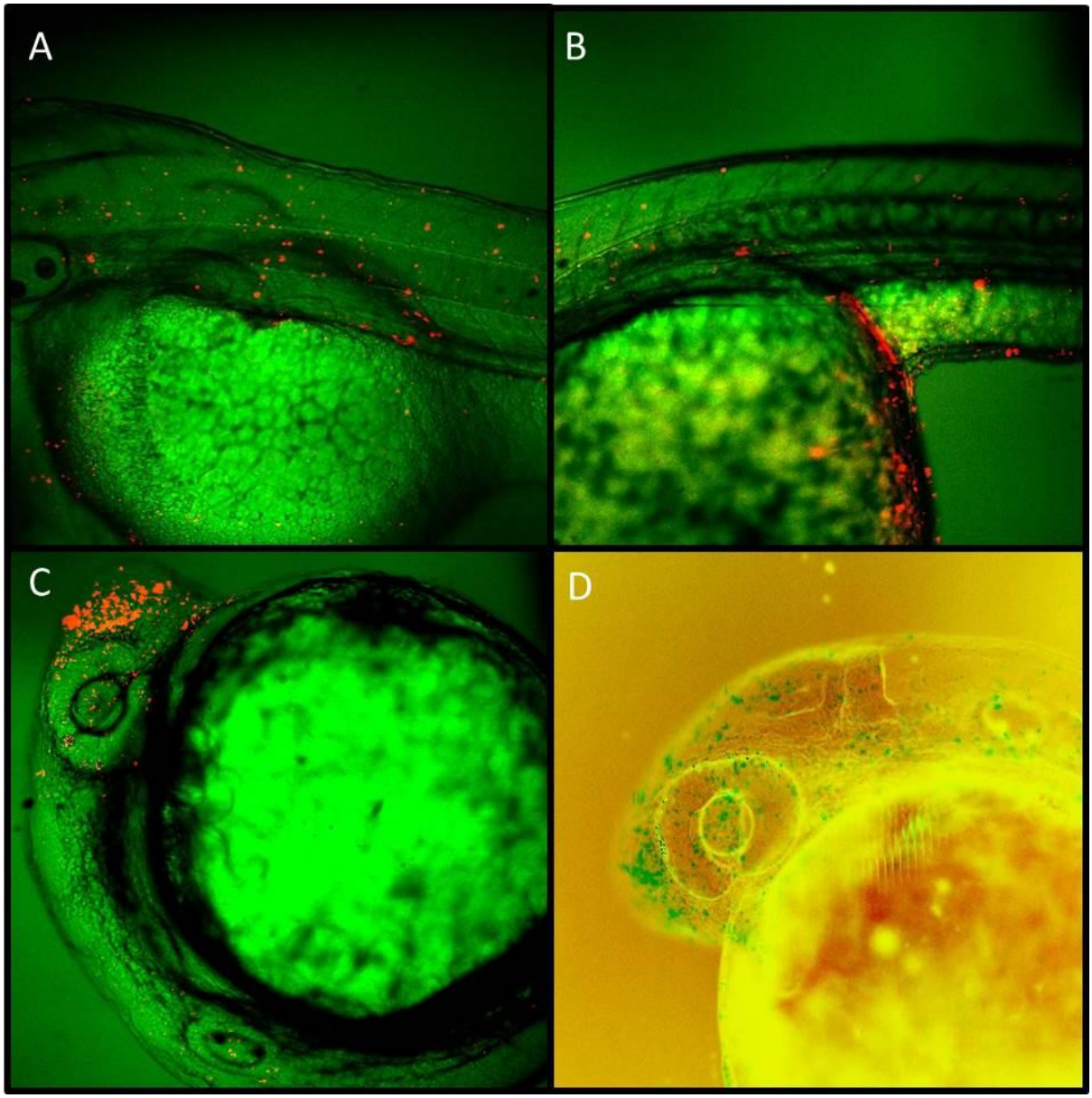

Figure 5. CARS images of zebrafish microinjected with Ag MNMs at the 1 cell stage. A) 48 hpf, associating indiscriminately with the trunk and tail. B) 24 hpf associating with the yolk sac. C) 23 hpf, MNMs bioconcentrated in the head region. D) 24 hpf distribution of the Ag MNMs throughout the rostral embryo. Particle aggregates are indicated in red in images A, B and C and green in D.

Stimulated raman scattering (SRS) was also trialled with some success to gain cleaner images, with reduced background interference from the sample (Figure 7). Practical disadvantages include the set-up being more time consuming and images only taken at high magnification, with reduced capability to have a large proportion of the embryo visualized at the same time. Sample thickness is a more important consideration with this technique and, due to the dipping lens required to gain sufficient collection of the CARS signal, the sample preparation required terminating the animals.

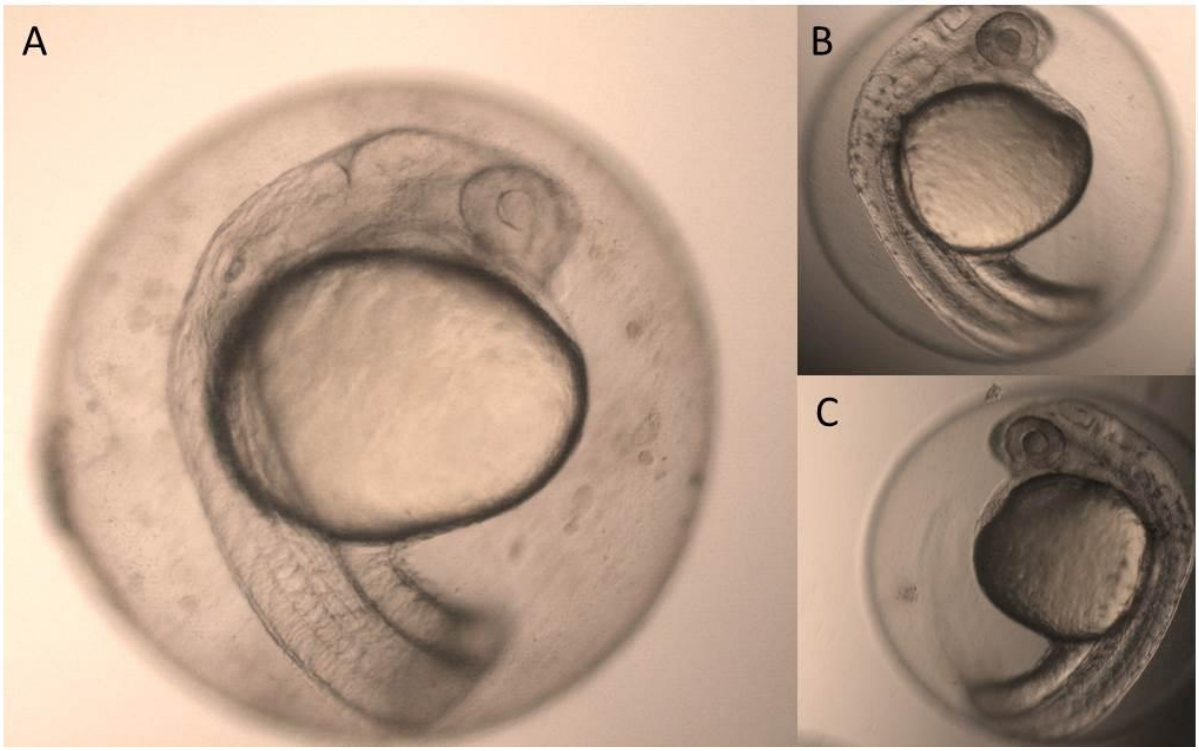

Figure 6. A) Zebrafish embryo exposed from 12 hpf to 26 hpf to 754 µM phenylthiourea (PTU). B,C) unexposed control embryos at the same age, showing the beginning of pigmentation process.

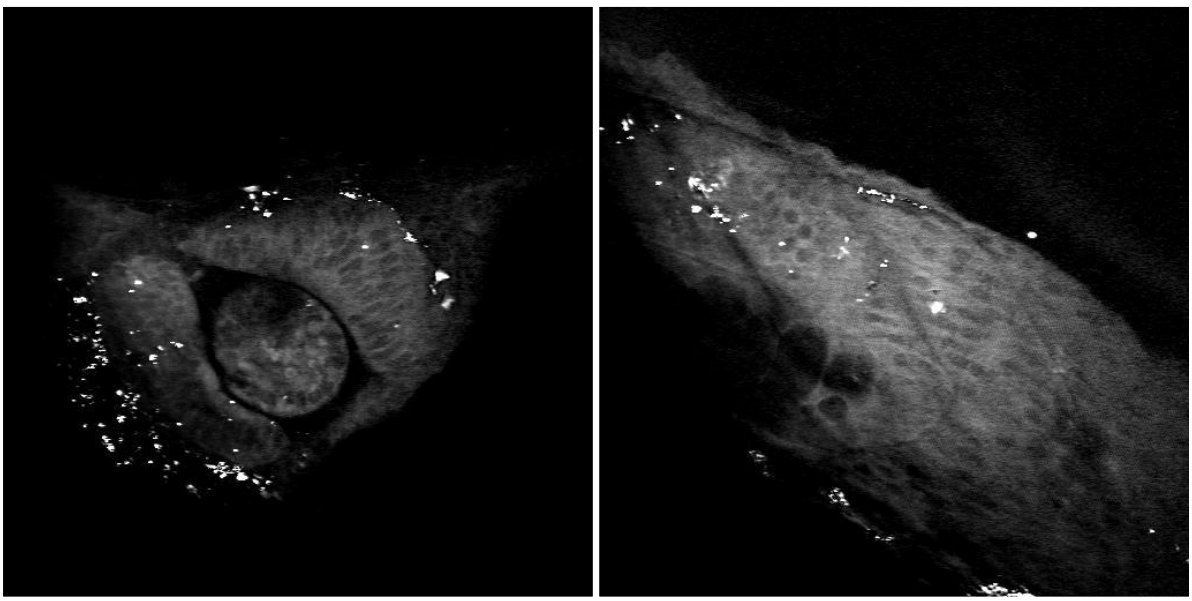

Figure 7. Stimulated raman scattering (SRS) images of 24 hpf embryo microinjected with Ag MNMs showing A) the eye region and B) the somatic muscle in the tail. SRS gains cleaner images due to the reduced background interference from the sample. Disadvantages of this approach included that images could only be taken at high magnification, thus limiting the area of the embryo that is visualized, and the set-up was more time consuming and sampling of the animal was terminal.

When applying CARS to waterborne exposures of zebrafish embryos to Ag MNMs, it was established that most (possibly all) of the particles accumulated on the surface coating of the chorion, with no direct evidence for penetration to the embryo. CARS imaging provided evidence for aggregation of the Ag MNMs (Figure 8, Osborne *et al.,* 2012). This finding was also the case for exposures to other metal based MNMs, including TiO_2 and ZnO.

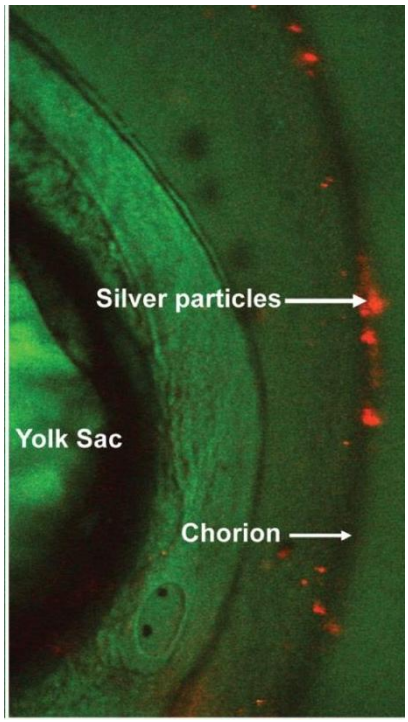

Figure 8. Coherent Anti-stokes Raman Scattering image of embryo exposed to silver nanoparticles after 24 h. Aggregates/agglomerates of nanoparticles appear as coloured (yellow/red) patches. CARS revealed nanomaterial on the surface of the chorion, likely as aggregates of nanoparticles but none were detected internally to the chorion, or within the embryo itself (Reproduced from Osborne *et al*. 2012).

We thus show that information derived from CARS can enable intelligent extrapolation on MNM fate based on direct imaging data. CARS imaging lends itself particularly well to imaging with embryos, such as for the zebrafish, where whole organism imaging can provide comprehensive assessment of nanoparticle fate and behaviour over early, and often the most sensitive stage of development (up to 48 hours post fertilisation).

4.2.2 WISH

Before it was possible to use specific target genes for informing on the target tissues for MNMs exposure effects, it was first necessary to establish the ontogeny profiles for expression of these genes using WISH.

Expression of target genes in zebrafish during early life (0-12 dpf):

mt2 (metallothionein 2) was expressed at 3-4 hpf in cells of the blastoderm, and then at a relatively low level at 24 hpf in the extended yolk sac region of the embryo. No expression was seen after 2 dpf up to 12 dpf (Figure 9, Ai-Aii).

gstm1 (glutathionine S-transferase mu) gave a low-level expression at 3-4 hpf in cells of the blastoderm which was more intense at 8-10 hpf. Low detectable expression of this gene occurred at 24 hpf in the extended yolk sac region. No detectable expression occurred during the subsequent development up to 12 dpf (Figure 9, Bi-Bii).

gstp (glutathionine S-transferase pi) expression was detected throughout the ontogeny period studied and was seen in olfactory bulbs, ventricles in the brain, neuromasts, jaw fins and gut. The patterns of expression and intensity of expression differed over the life stages studied. At 24 hpf gstp expression was seen in the extended yolk sac region and at 48 hpf in the olfactory bulbs and brain ventricles. At 3 dpf expression was seen in neuromasts expressed along the lateral line and at 96 hpf also in the jaw. At 3 dpf some weak expression also occurred in the region of the olfactory bulb. Gstp expression was seen in the pectoral fins at 120 hpf, and at 144 hpf was also associated with the region of the gut. At 168 hpf, 192 hpf and 240 hpf there was relatively weak *gstp* expression and this was seen predominantly in neuromasts (Figure 9, Ci-Cviii).

hmox 1 (heme oxygenase 1) showed little detectable expression of *hmox1* in embryos until 24 hpf, when a relatively high level of expression was observed in the retina and at the tip of extended yolk sac. At 48 hpf expression also occurred in the retina, in the yolk sac and in some neuromasts. At 72 hpf onwards some (18%) of the embryos studied showed a low level, or no observable expression of hmox1, until 7 dpf when there was a relatively high level expression in the liver (Sadler *et al*., 2007) which was continued subsequently to 12 dpf (Figure 10, Di-Dvii).

Expression of *fth1* (ferritin heavy chain 1) occurred 3-4 hpf in the entire blastoderm. At 7-9 hpf low level expression was detected in the germ ring and at 24 hpf there was a pronounced expression in the forebrain, which persisted in the brain at 48 hpf with additional expression in the extended yolk sac. No expression of fth1 was detected at 72 hpf or at 96 hpf, but from day 6 to 11 variable and relatively low level expression occurred in the yolk sac and/or gills. *Fth1* expression occurred in the liver from 144 hpf to 216 hpf, was absent in this tissue at 240 hpf, but detected again at 264 hpf (Figure 9, Ei-Eviii).

Based on the ontogeny of expression of the different genes, appropriate life stages were chosen for exposure studies on Ag MNMs. These stages allowed for analysis assessing possible stimulation and/or suppression of target gene expression. *Mt2*: 24 hpf and 4 dpf, *gstp*: 24 hpf, 48 hpf and 4 dpf, *hmox*1 and *fth1*: 24 hpf and 5 dpf, *gstm1*: 24 hpf, 4 dpf and 5 dpf.

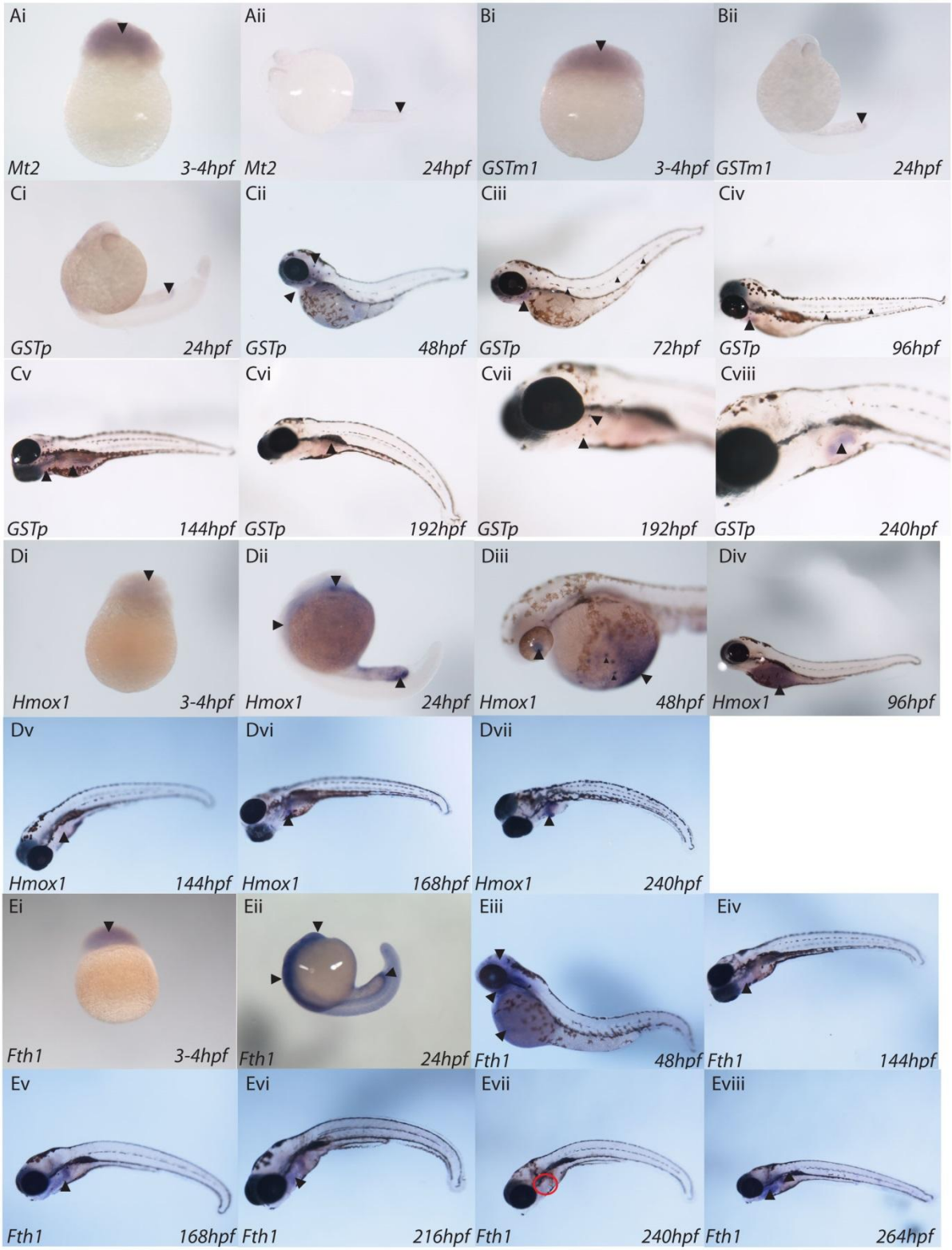

Figure 9. Representative in situ hybridisation images showing ontogeny of expression of *Mt2, GSTp, GSTm1, Fth1* and *Hmox1* for up to 12 dpf in zebrafish: *Mt2* in 3-4hpf (Ai) and 24hpf (Aii) embryos; *GSTm1* in 3-4hpf (Bi) and 24hpf (Bii) embryos; *GSTp* in a 24hpf (Ci), 48hp, (Cii), 72hpf (Ciii) 96hpf (Civ) 144hpf (Cv), 192hpf (Cvi, and CVii with head close up, showing neuromasts , and 240hpf (Cviii,

showing extended yolk sac) embryos/larvae ; Hmox1 in 3-4hpf (Di), 24hpf (Dii), 48hpf (Diii) 96hpf (Div), 144hpf (Dv) 168hpf (Dvi), and 240hpf (Dvii) embryos/larvae; Fth1 in 3-4hpf (Ei), 24hpf (Eii), 48hpf (Eiii), 144hpf (Eiv), 168hpf (Ev), 216hpf (Evi), 240hpf (Evii) and 264hpf (Eviii) embryos/larvae. Arrowheads indicate focal areas of expression for the target genes studied.

Effects of silver materials on gene expression

mt2

At 24 hpf, in non-exposed embryos 57% showed a detectable expression of *mt2* in the extended yolk sac region and this was consistently elevated (80% + embryos) for waterborne exposures to 500 µg AgNPCi (10nm citrate coated)/l (4.6-fold), 500 µg AgBCi (160nm, bulk citrate coated)/l (4.7-fold) and 20 µg $AgNO_3$/l (2.7-fold) (Figure 10, Ai-Av). At 4 dpf (Figure 9 Bi-Bii) a 24-hour exposure to AgNPCi resulted minimally in a 2-fold higher level of mt2 expression across various regions of the larval body including head, jaw and yolk sac (and consistently so, in 92% of the embryos). All silver treatments induced mt2 and there was a concentration dependent response to the silver materials for *mt2* (Figure 10), principally in the region of the extended yolk sac (Figure 10 Ai-Aiv).

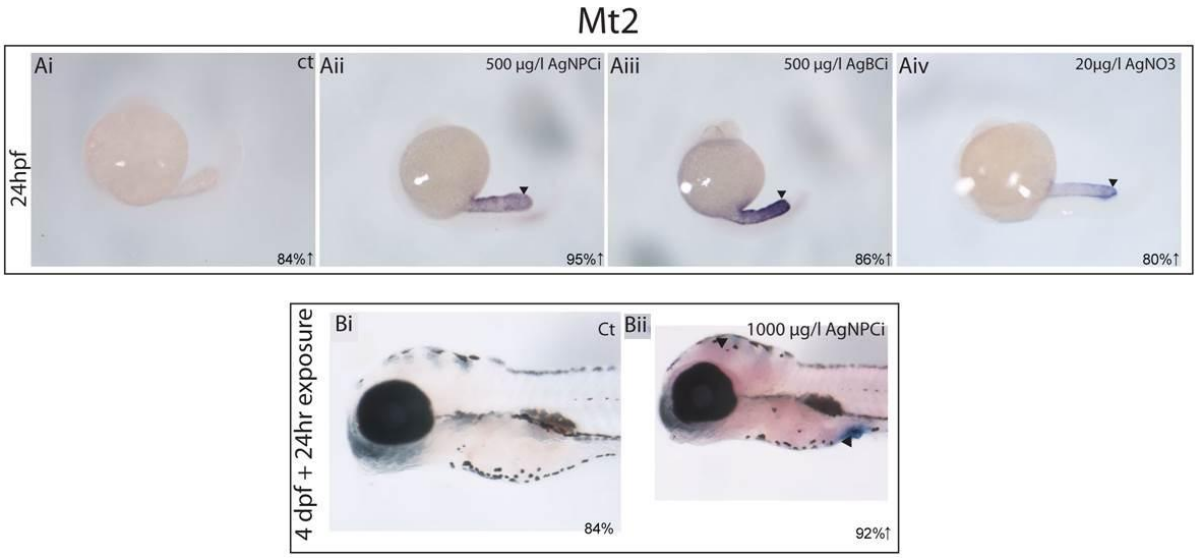

Figure 10. Expression of *mt2* in zebrafish embryos/larvae at 24 hpf-after 24h of exposure to AgNPCi, AgBCi and $AgNO_3$ as determined by whole mount *in situ* hybridisation. ▲ Indicates target tissue/focal areas where *mt2* expression was affected by the treatments. Ai. Control embryo, Aii. 500 µg AgNPCi/l, Aiii. 500 µg AgBCi/l, Aiv. 20 µg $AgNO_3$/l (all 24 hours post fertilisation). Bi-ii, Bi. Control larvae, Bii 1000 µg/l AgNPCi (all exposed at 4 days post fertilisation for 24 h..

gstp

At 24 hpf gstp expression was enhanced in the extended yolk sac by between 1.5 and 1.7-fold above controls for exposures to 500 µg AgNPCi/l, 500 µg AgBCi/l and 20 µg $AgNO_3$/l, and in a consistent manner (more than 90% of the embryos responding in the same manner) (Figure 11 A, B). For ionic

silver, there were 1.5-fold and 1.6-fold higher levels of expression in the head and pectoral fin, respectively (Figure 11 Ci). Antibody staining of ionocytes with vHATPase (shown in green) NakATPase (shown in red, Figure 11 Di-Div) showed that focal areas of *gstp* expression on the yolk sac, extended yolk sac and some other body regions of zebrafish larvae were co-localised with vHATPase and NakATPase skin cells. In 4 dpf larvae, (Figure 11 Ei-Eii) 24-h exposure to AgNPCi (1000 µg/l) resulted in a 2-fold higher expression of *gstp* across various body of the larvae (and in 100% of the embryos examined). *Gstp* expression induced by Ag materials in a variety of tissues is consistent with findings from previous studies showing oxidative stress in fish exposed to Ag MNMs (Choi *et al*., 2009, Foldbjerg et al., 2009). Induction of this gene was also seen in olfactory bulbs, an established tissue target for heavy metals and potentially affecting olfaction (Gobba, 2006).

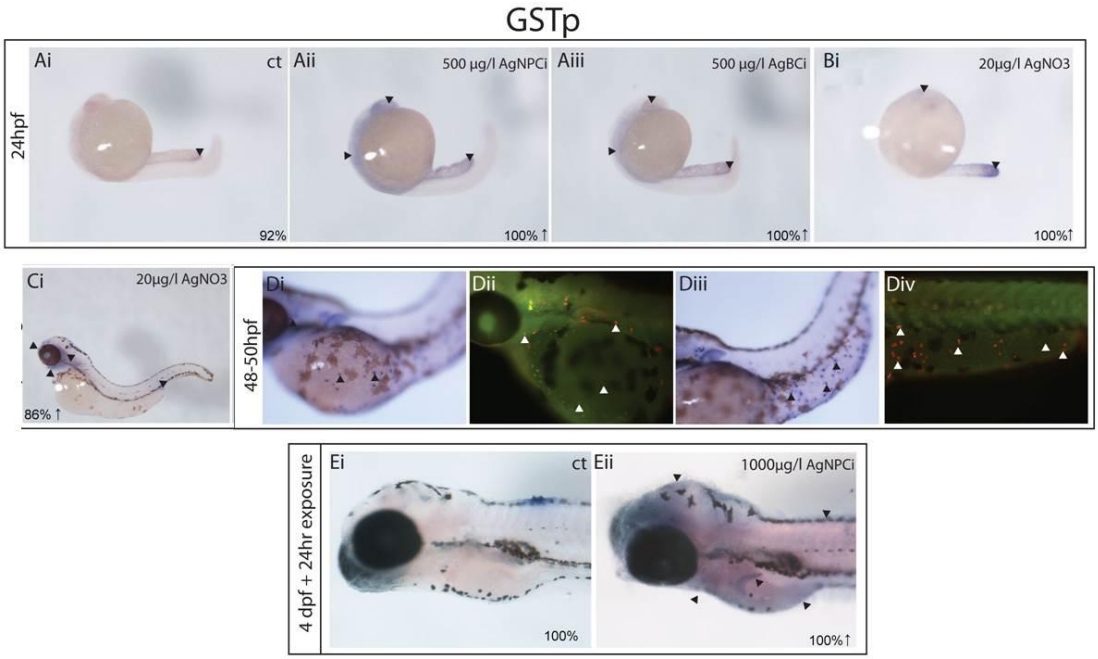

Figure 11. Expression of *gstp* in zebrafish embryos/larvae at 24 hpf-after exposure to AgNPCi, AgBCi and $AgNO_3$ as determined by whole mount *in situ* hybridisation. ▲ Indicates target tissue/focal areas where *gstp* expression was affected by the treatments. Ai. Control embryo, Aii. 500 µg AgNPCi/l, Aiii. 500 µg AgBCi/l, Bi. 20 µg $AgNO_3$/l (all 24 hours post fertilisation). Di-Div Embryos exposed to AgMNMs and subjected to *in situ* hybridisation for *gstp* and antibody staining with vHATPase (green) and NaKATPase (red) to detect ionocytes. Di. Exposure to 500 µg AgNP/l showing *in-situ* staining at 50 hpf, Dii. Close up of embryo at 50 hpf after application of antibody staining (green -vHATPase, and red -NaKATPase) to reveal ionocytes on yolk sac, Diii. 500 µg AgNP/l dosed embryo showing skin cell staining on extended yolk sac, Div. embryo after application of antibody staining (green -vHATPase, red -NaKATPase) indicating ionocytes on yolk sac. Ei-ii, Ei. Control larvae, Eii 1 000 µg/l AgNPCi (all exposed at 4 days post fertilisation for 24 h).

gstm1

At 24 hpf *gstm1* was expressed in controls (57% of the embryos) at detectable (albeit low) levels in the extended yolk sac region. Exposure to 500 µg AgNPCi/l, 500 µg AgBCi/l and 20 µg $AgNO_3$/l

induced enhanced expression between 1.6 and 1.8–fold higher in the extended yolk sac region. AgNPCi and AgBCi induced between 1.2 and 1.8–fold higher expression in the head region (occurring in over 60% of embryos). The same pattern occurred for exposures to $AgNO_3$ but with higher fold inductions (4.8-fold in the head for 40% of the embryos). At 4 dpf larvae showed a consistently (70% of the embryos) enhanced expression of *gstm1* for exposures to 1000 µg AgNPCi/l, 1000 µg AgBCi/l and 20 µg AgNO3/l with focal activity in regions of the head (between a 1.9 and 2.1 fold increase) and yolk sac (between 1.2-1.7-fold increase). There was no detectable expression of *gstm1* in control embryos (Figure 4 Bi-Biv).

hmox1

At 24 hpf there was no effect of any of the silver treatments (AgNPCi, AgBCi nor $AgNO_3$) on the expression of *hmox1* in the yolk sac region or the lens region of the eye (Figure 12 Ai-Aiv). At 5 dpf, hmox1 expression was down regulated in all of the larvae in the head region (0.5 fold of controls) and yolk sac (0.7 fold of controls) (Figure 12 Bi-Bii).

fth1

At 24 hpf, fth1 expression occurred mainly in the head and in almost all (97%) of control embryos (Figure 12 Ci-Civ). There was also some more minor expression seen on the skin. There were no obvious effects of exposure to AgNPCi, AgBCi nor $AgNO_3$ on the expression pattern or intensity for fth1 compared to controls. However, at 5 dpf a 6 h exposure to AgNPCi (1000 µg/l) resulted in a suppressive effect (in all larvae) on the expression of fth1 in both the head and yolk sac region (expression was between 0.4 and 0.5 fold of controls; Figure 12Di-Dii).

Oxidative stress (occurring through ROS) and inflammatory responses have been shown also to have suppressive effects on *hmox1* in mice, for example in chronic inflammatory illness (Poss and Tonegawa, 1997). The reduced expression of both *hmox1* and *fth1* in the head region and yolk sac after a 6-hour exposure to AgNPCi s in 5 dpf zebrafish may follow a similar pathway. Intracellular excess iron causes oxidative stress by generating Fe^{2+} and in turn a hydroxyl radical in the Fenton reaction (Harrison and Arosio, 1996). It is still uncertain whether ferritin causes more oxidative stress by releasing Fe^{2+} as part of its cytoprotective role of oxidative stress (Arosio *et al*., 2009). It has been suggested that this is why *fth1* down-regulation or over expression can be seen during oxidative stress (Orino and Watanabe, 2008). In our study we observed a suppressed effect of AgMNM on *fth1* expression (Figure 12 Di-Dii).

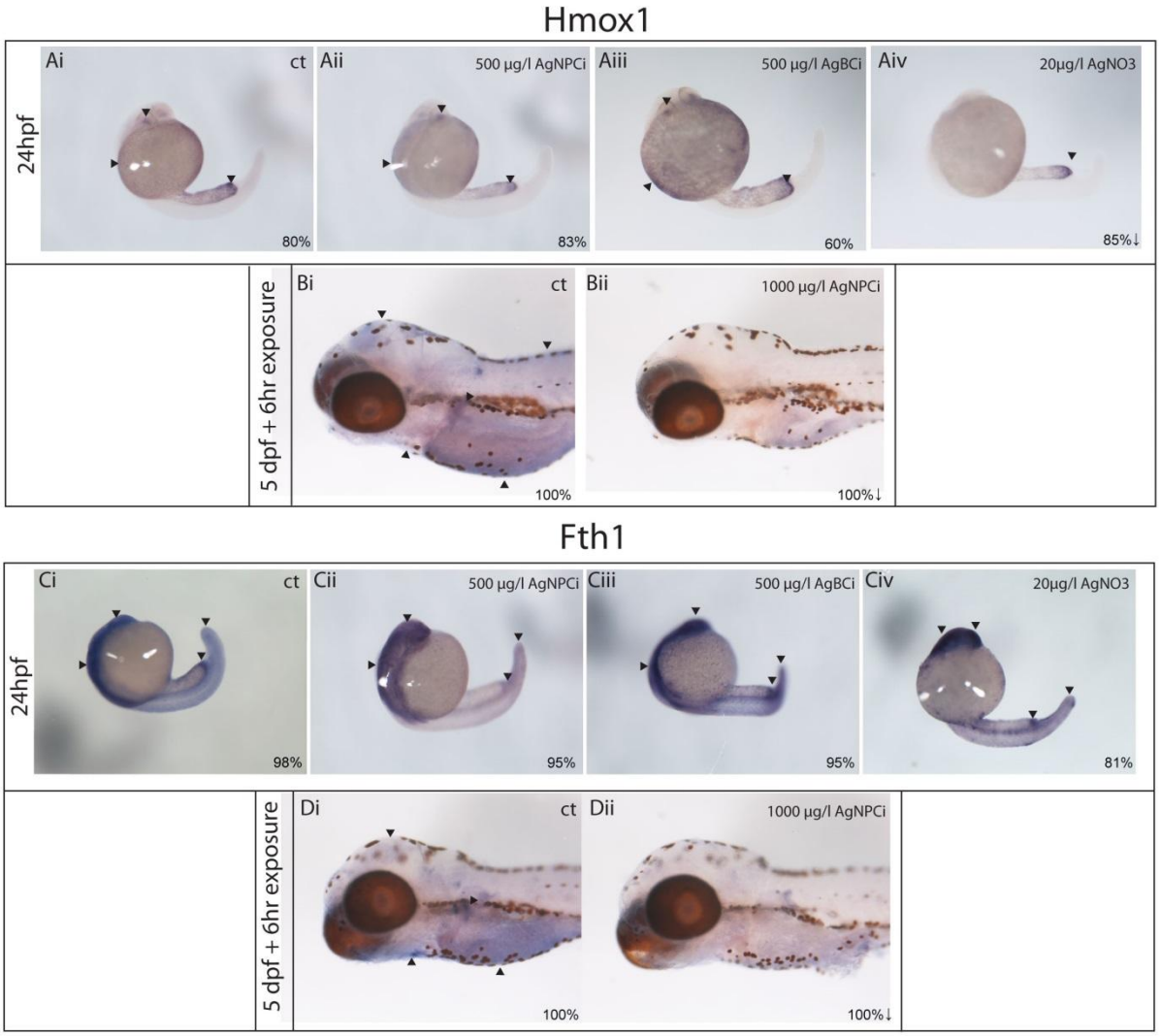

Figure 12. Expression of *hmox1* and *fth1* in zebrafish embryos/larvae at 24 hpf-after exposure to coated AgNPCi, AgBCi and $AgNO_3$ as determined by whole mount in situ hybridisation. ▲ Indicates target tissue/focal areas of *hmox1* and *fth1* expression. *Hmox1*: Ai. Control embryo, Aii. 500 µg AgNPCi/l, Aiii. 500 µg AgBCi/l, Aiv. 20 µg $AgNO_3$/l (all 24 hours post fertilisation). Bi-ii, Bi. Control larvae, Bii 1 000 µg/l AgNPCi (all exposed at 5 days post fertilisation for 6 h). *Fth1*: Ci. Control embryo, Cii. 500 µg AgNPCi/l, Ciii. 500 µg AgBCi/l, Civ. 20 µg $AgNO_3$/l (all 24 hours post fertilisation). Di-ii AgNPCi, Di. Control larvae, Dii 1 000 µg/l (all exposed at 5 days post fertilisation for 6 h). Numbers represent percentage of embryos affected in the treatment (n = 15-20). Upwards and downwards pointing arrows indicate enhanced or reduced gene expression respectively compared with controls.

5. Conclusions and recommendations

Here we have developed and applied a series of methods to study the uptake and localisation of MNMs in isopods and zebrafish, as model test species, to facilitate studies into the bioavailability of

MNMs to ecotoxicology species. Atomic absorption spectrometry (AAS) and proton induced X-ray emission (PIXE) analysis were applied (UNI-Lj) to determine uptake and tissue concentration for selected MNMs and/or ions derived from these materials and quantitative elemental concentration maps of biological tissue produced in the isopod, *P. scaber.* This work established that TiO_2 MNMs do not accumulate in intact digestive gland cells, but for Ag MNM exposures, silver co-localises with Cu in metal storing granules of the digestive gland. From this we can conclude that Ag^+ ions rather than Ag MNMs particles entered the cells of the digestive gland. The overlapping profiles of silver and copper for the elemental distribution indicates that silver follows the same cellular pathways as other metal ions, such as Cu^{2+} which are transported to metal storage granules where they accumulate.

CARS was applied successfully to both early and late embryonic life stage zebrafish embryos and the data presented further illustrate the potential of CARS microscopy as a powerful tool for supporting other techniques to help trace MNM uptake and distribution and inform on MNM toxicology within cellular and tissue matrices. Furthermore, the method lends itself to analysis in real time and on live samples. Using this method, we show that uptake of MNMs from the exposure medium into zebrafish embryos is minimised by particle aggregation and the low permeability of the chorion. It needs to be recognised however that CARS as a technique currently does have some inherent limitation for application to studies on MNMs, including resolution and the fact that it is qualitative only (see Goodhead et al., 2014 for further discussion).

Applying WISH for selected genes known to play key roles in metal trafficking and oxidative metabolism, target tissues for silver nanomaterial effects in exposed zebrafish embryos have been clearly identified and they include tissues involved in environmental sensing (olfactory bulbs and neuromasts) and ionocytes involved with ion transport. The gene responses associated with detoxification and oxidative stress however appear to occur as a consequence of silver ions rather than a physical feature of the silver nanomaterials tested, albeit more work would be needed to verify this fully.

6. References

Akimov D, Chatzipapadopoulos S, Meyer T, Tarcea N, Dietzek B, Schmitt M, et al. Different contrast information obtained from CARS and nonresonant FWM images. Journal of Raman Spectroscopy 2009; 40: 941-947.

Andrews, G. K. Regulation of metallothionein gene expression by oxidative stress and metal ions. Biochemical pharmacology; 2000: 59, 95-104.

Arosio, P., Ingrassia, R. & Cavadini, P. Ferritins: a family of molecules for iron storage, antioxidation and more. Biochimica et Biophysica Acta (BBA)-General Subjects; 2009: 1790, 589-599.

Bings NH, Bogaerts A and Broekaert JAC. Atomic spectroscopy. Analytical Chemistry; 2006: 78, 3917-3945

Cheng C, Porter AE, Muller K, Koziol K, Skepper JN, Midgley P, et al. Imaging carbon nanoparticles and related cytotoxicity. In: Kenny L, editor. Inhaled Particles X. 151, 2009a.

Cheng J, Flahaut E, Cheng S, H. Effect of carbon nanotubes on developing zebrafish (Danio rerio) embryos. Environmental Toxicology and Chemistry 2007; 26: 708-716.

Cheng JP, Chan CM, Veca LM, Poon WL, Chan PK, Qu LW, et al. Acute and long-term effects after single loading of functionalized multi-walled carbon nanotubes into zebrafish (Danio rerio). Toxicology and Applied Pharmacology 2009b; 235: 216-225.

Cheng JX, Jia YK, Zheng GF, Xie XS. Laser-scanning coherent anti-stokes Raman scattering microscopy and applications to cell biology. Biophysical Journal 2002b; 83: 502-509.

Cheng J-X, Volkmer A, Xie XS. Theoretical and experimental characterization of coherent anti-Stokes Raman scattering microscopy. J. Opt. Soc. Am. B 2002a; 19: 1363-1375.

Cheng, W., Guo, L., Zhang, Z., Soo, H. M., Wen, C., Wu, W. & Peng, J. HNF factors form a network to regulate liver-enriched genes in zebrafish. Developmental biology; 2006: 294, 482-496.

Choi, J. E., Kim, S., Ahn, J. H., Youn, P., Kang, J. S., Park, K., Yi, J. & Ryu, D. Y. Induction of oxidative stress and apoptosis by silver nanoparticles in the liver of adult zebrafish. Aquatic Toxicology; 2009: 100, 151-159.

Drobne D. Terrestrial Isopods—A Good Choice for Toxicity Testing of Pollutants in the Terrestrial Environment. Environmental Toxicology and Chemistry; 1997: 16, 1159–1164.

Drobne D., Hopkin S.P. Ecotoxicological laboratory test for assessing the effects of chemicals on terrestrial isopods. Bulletin of Environmental Contamination and Toxicology; 1995: 53: 390–397.

Drobne D., Hopkin S.P. The Toxicity of Zinc to Terrestrial Isopods in a »Standard« Laboratory Test. Ecotoxicology and Environmental Safety; 1994: 31, 1–6

Fabrega J, Luoma SN, Tyler CR, Galloway TS and Lead JR. Silver nanoparticles: Behaviour and effects in the aquatic environment. Environment International; 2011: 37, 517-531.

Fan Q-L, Neoh K-G, Kang E-T, Shuter B, Wang S-C. Solvent-free atom transfer radical polymerization for the preparation of poly(poly(ethyleneglycol) monomethacrylate)-grafted Fe3O4 nanoparticles: Synthesis, characterization and cellular uptake. Biomaterials 2007; 28: 5426-5436.

Ferry JL, Craig P, Hexel C, Sisco P, Frey R, Pennington PL, et al. Transfer of gold nanoparticles from the water column to the estuarine food web. Nat Nano 2009; 4: 441-444.

Foldbjerg, R., Olesen, P., Hougaard, M., Dang, D. A., Hoffmann, H. J. & Autrup, H. PVP-coated silver nanoparticles and silver ions induce reactive oxygen species, apoptosis and necrosis in THP-1 monocytes. Toxicology letters; 2009: 190, 156-162.

Garner, L. V. & Di Giulio, R. T. Glutathione transferase pi class 2 (GSTp2) protects against the cardiac deformities caused by exposure to PAHs but not PCB-126 in zebrafish embryos. Comparative Biochemistry and Physiology Part C: Toxicology & Pharmacology; 2012: 155, 573-579.

Garrett N, Whiteman M, Moger J. Imaging the uptake of gold nanoshells in live cells using plasmon resonance enhanced four wave mixing microscopy. Opt. Express 2011; 19: 17563-17574.

Gobba, F. Olfactory toxicity: long-term effects of occupational exposures. International archives of occupational and environmental health; 2006: 79, 322-331.

Hames C.A.C., Hopkin S.P. The structure and function of the digestive system of terrestrial isopods. Journal of Zoology; 1989: 217, 4, 599–627

Hashimoto M, Araki T, Kawata S. Molecular vibration imaging in the fingerprint region by use of coherent anti-Stokes Raman scattering microscopy with a collinear configuration. Optics Letters 2000; 25: 1768-1770.

Johnston HJ, Semmler-Behnke M, Brown DM, Kreyling W, Tran L, Stone V. Evaluating the uptake and intracellular fate of polystyrene nanoparticles by primary and hepatocyte cell lines in vitro. Toxicology and Applied Pharmacology 2010; 242: 66-78.

K. Vogel-Mikuš, P. Pongrac, P. Pelicon, P. Vavpetič, B. Povh, H. Bothe, M. Regvar, Micro-PIXE analysis for localisation and quantification of elements in roots of mycorrhizal metal-tolerant plants, in: A. Varma, A.C. Kharkwal (Eds.), Symbiotic Fungi: Principles and Practice, (Soil biology, 18), Springer, Heidelberg, 2009, p. 227.

Larner F, Dogra Y, Dybowska A, Fabrega J, Stolpe B, Bridgestock LJ, et al. Tracing Bioavailability of ZnO Nanoparticles Using Stable Isotope Labeling. Environmental Science & Technology 2012; 46: 12137-12145.

Lu K, Zhang ZY, He XA, Ma YH, Zhou KB, Zhang HF, et al. Bioavailability and Distribution and of Ceria Nanoparticles in Simulated Aquatic Ecosystems, Quantification with a Radiotracer Technique. Journal of Nanoscience and Nanotechnology 2010; 10: 8658-8662.

Maracine M, Segner H. Cytotoxicity of metals in isolated fish cells: Importance of the cellular glutathione status. Compar Biochem Physiol. 1998; 120A:83–88.

Mason AZ, Jenkins KD. Metal detoxification in aquatic organisms. In: Tessier A, Turner DR, editors. Metal Speciation and Bioavailability in Aquatic Ecosystems. New York, NY: Wiley; 1995. pp. 478–608.

Mouchet F, Landois P, Sarremejean E, Bernard G, Puech P, Pinelli E, et al. Characterisation and in vivo ecotoxicity evaluation of double-wall carbon nanotubes in larvae of the amphibian Xenopus laevis. Aquatic Toxicology 2008; 87: 127-137.

Novak S, Drobne D, Valant J, Pipan-Tkalec Z, Pelicon P, Vavpetic P, Grlj N, Falnoga I, Mazej D and Remskar M. Cell membrane integrity and internalization of ingested TiO2 nanoparticles by digestive gland cells of a terrestrial isopod. Environmental Toxicology and Chemistry; 2012: 31, 1083-1090.

Orino, K. & Watanabe, K. Molecular, physiological and clinical aspects of the iron storage protein ferritin. The Veterinary Journal; 2008: 178, 191-201.

Osborne, O. J., Johnston, B., Moger, J., Baalousha, M., Lead, J., Kudoh, T. & Tyler, C. Effects of particle size and coating on nanoscale Ag and TiO2 exposure in zebrafish (Danio rerio) embryos. Nanotoxicology; 2012: 1-34.

Petri-Fink A, Steitz B, Finka A, Salaklang J, Hofmann H. Effect of cell media on polymer coated superparamagnetic iron oxide nanoparticles (SPIONs): Colloidal stability, cytotoxicity, and cellular uptake studies. European Journal of Pharmaceutics and Biopharmaceutics 2008; 68: 129-137.

Pipan Tkalec Z, Drobne D, Vogel-Mikus K, Pongrac P, Regvar M, Strus J, Pelicon P, Vavpetic P, Grlj N and Remskar M. Micro-PIXE study of Ag in digestive glands of a nano-Ag fed arthropod (Porcellio scaber, Isopoda, Crustacea). Nuclear Instruments & Methods in Physics Research Section B-Beam Interactions with Materials and Atoms; 2011: 269, 2286-2291.

Ponka, P., Beaumont, C. & Richardson, D. R. Year. Function and regulation of transferrin and ferritin. In: Seminars in hematology, 1998. 35.

Poss, K. D. & Tonegawa, S. Heme oxygenase 1 is required for mammalian iron reutilization. Proceedings of the National Academy of Sciences, 94; 1997: 10919-10924.

Scown TM, Goodhead RM, Johnston BD, Moger J, Baalousha M, Lead JR, et al. Assessment of cultured fish hepatocytes for studying cellular uptake and (eco)toxicity of nanoparticles. Environmental Chemistry 2010; 7: 36-49.

Soto KF, Carrasco A, Powell TG, Garza KM, Murr LE. Comparative in vitro cytotoxicity of some manufactureed nanoparticulate materials characterized by transmission electron microscopy. Journal of Nanoparticle Research 2005; 7: 145-169.

Sumner SCJ, Fennell TR, Snyder RW, Taylor GF, Lewin AH. Distribution of carbon-14 labeled C60 ([14C]C60) in the pregnant and in the lactating dam and the effect of C60 exposure on the biochemical profile of urine. Journal of Applied Toxicology 2010; 30: 354-360.

Volkmer A, Cheng JX, Xie XS. Vibrational imaging with high sensitivity via epidetected coherent anti-Stokes Raman scattering microscopy. Physical Review Letters 2001; 87.

Xu P, Gullotti E, Tong L, Highley CB, Errabelli DR, Hasan T, et al. Intracellular Drug Delivery by Poly(lactic-co-glycolic acid) Nanoparticles, Revisited. Molecular Pharmaceutics 2008; 6: 190-201.